APPLIED PHYSICS LETTERS **91**, 072905 (2007)

Probing fatigue in ferroelectric thin films with subnanometer depth resolution

Jiang-Li Cao[a)]
II Physikalisches Institut B, RWTH Aachen University, D-52056 Aachen, Germany and Department of Materials Physics and Chemistry, University of Science and Technology Beijing, 100083 Beijing, China

Axel Solbach and Uwe Klemradt
II Physikalisches Institut B, RWTH Aachen University, D-52056 Aachen, Germany

Thomas Weirich and Joachim Mayer
Gemeinschaftslabor für Elektronenmikroskopie, RWTH Aachen University, D-52074 Aachen, Germany

Peter J. Schorn and Ulrich Böttger
Institut für Werkstoffe der Elektrotechnik II, RWTH Aachen University, D-52056 Aachen, Germany

(Received 4 June 2007; accepted 24 July 2007; published online 15 August 2007)

The authors report the study of polarization fatigue in $Pb(Zr,Ti)O_3$ (PZT) ferroelectric thin films using *in situ* high-resolution grazing incidence x-ray specular reflectivity of synchrotron radiation. The results demonstrate that there is no formation of a region of different electron densities in the film growth direction with subnanometer depth resolution during fatigue. The upper bounds on the theoretically predicted interfacial accumulation of oxygen vacancies at the interfaces between PZT and Pt electrodes are determined by the comparison of experimental results and theoretical simulations. © *2007 American Institute of Physics*. [DOI: 10.1063/1.2771534]

Perovskite (ABO_3) ferroelectric oxides have triggered much attention due to their broad potential applications in the next generation of information technology electronics, such as ferroelectric memories and logic devices, owing to their two nonvolatile polarization states.[1–3] The nonvolatility of polarization in ferroelectric materials is termed due to the two stable polarization states, which is derived from the switching of the spontaneous polarization under external electric field and being frozen even after the interruption of the electric field. The two ferroelectric polarization states constitute the basic "0" and "1" of logic units. The development of practical ferroelectric devices is absolutely dependent on a robust nonvolatility.

However, polarization fatigue can lead to significant deterioration of the nonvolatility, resulting in the failure of the devices. Polarization fatigue represents the decrease of switchable polarization after repeated switching under an external alternating-current (ac) electric field.[1–10] It is the most challenging reliability issue for these ferroelectric components. Currently, the increasing accumulation of positively charged oxygen vacancies to the ferroelectric/electrode interfaces is theoretically assumed to be responsible for polarization fatigue. However, so far the microscopic structural aspects of the interfacial oxygen vacancy accumulation have not been fully understood. A vast amount of work has been carried out based on this theoretical understanding to develop fatigue models, e.g., the structural lattice distortion and domain wall pinning. Nevertheless, the improvement for controlling fatigue in $Pb(Zr,Ti)O_3$ (PZT) thin films with metal electrodes is limited.

In the present study, *in situ* high-resolution grazing incidence x-ray specular reflectivity (XRSR) of synchrotron radiation was adopted to investigate the structural evolution in ferroelectric thin film capacitors during fatigue. XRSR is a Fourier transform of the spatial distribution of the electron density profile perpendicular to the sample surface.[11] It has a depth resolution of subnanometer, while the inspected sample area is on a macroscopic scale, which makes it ideally suitable for structural observation of two-dimensional nanofilms. The highly parallel and brilliant x rays of synchrotron radiation enable the structural information of deeply buried structures in the sample to be accessible.

$Pb(Zr_{0.3}Ti_{0.7})O_3$ thin film capacitors with Pt electrodes were used as the model system. The (100)-preferentially oriented PZT thin films were deposited by a chemical solution deposition method on $Pt/TiO_x/SiO_2/Si$ substrates of 1×1 in.^{2} [12] Rectangular top Pt electrodes with a size of 4×2.2 mm^2 were prepared by dc-sputtering through UV photolithography and postannealed in pure oxygen. Then, a slice of the substrate with a capacitor in the center was cut out from the sample for *in situ* XRSR measurements. The PZT capacitors have a high-quality layered structure. The PZT film has a columnar grain structure in the thickness direction.[12] The d_{100} spacing of PZT is 3.992 Å as determined by x-ray diffraction measurement. A PZT thin film capacitor was used for the *in situ* XRSR investigation. A Sawyer-Tower setup was used for the measurements of the hysteresis loop and fatigue endurance.[13] The fatigue measurements were performed at room temperature by applying a triangular ac field (100 kHz and 8 V). After certain numbers of switching cycles, the hysteresis loops were measured using a triangular ac field (100 Hz and 8 V). *In situ* XRSR measurements were conducted on a high-resolution reflectometer using monochromatic synchrotron radiation at energy of 11 keV ($\lambda = 1.127$ Å) at HASYLAB (DESY).[12,13] A depolarization treatment to the PZT capacitor[14] was applied before each XRSR measurement to avoid interferences from imprint. It also means that the polarization was at zero level at

[a)]Author to whom correspondence should be addressed; FAX: +8610 6233 3649; electronic mail: jlcao@mater.ustb.edu.cn and cao@physik.rwth-aachen.de

 © 2007 American Institute of Physics
Downloaded 11 Feb 2009 to 131.169.95.132. Redistribution subject to AIP license or copyright; see http://apl.aip.org/apl/copyright.jsp

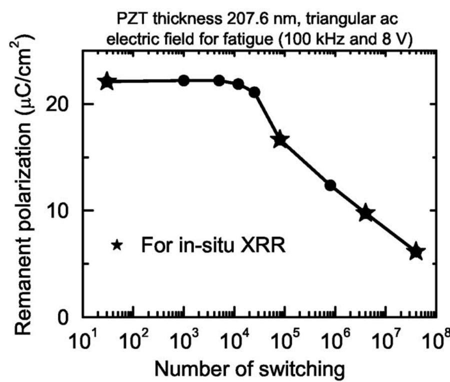

FIG. 1. Polarization fatigue. Remanent polarization of the PZT capacitor is plotted as a function of the switching cycles. The four fatigue states for the *in situ* XRSR measurements are marked.

each fatigue state for the *in situ* XRSR measurements. No deteriorating effects of the x rays on the capacitor were observed. More detailed description for the experimental procedures can be found in earlier works.[12,13]

Figure 1 illustrates the evolution of polarization fatigue of the PZT capacitor. The remanent polarization decreases rapidly after about 10^4 switching cycles from the virgin state of 22.1–6.1 $\mu C/cm^2$ at 4×10^7 switching cycles. The four fatigue states for the *in situ* XRSR measurements were marked in five-pointed star.

Figure 2 shows the *in situ* x-ray specular reflectivity of the PZT thin film capacitor corresponding to the four different fatigue states on a log scale as a function of the incidence angle. The specular reflectivity ranges eight orders of magnitude. There is hardly any difference among the XRSR curves except for the little higher fluctuation at high angles in curve A due to the measurement itself. Generally speaking, the x rays see the component layers in the capacitor in the thickness direction, layer by layer, with increasing incidence angle, as illustrated in the inset. Therefore, no heavily structurally distorted layer with a different electron density from PZT and no interface broadening are generated during fatigue. The experimental XRSR is fitted through the Parratt

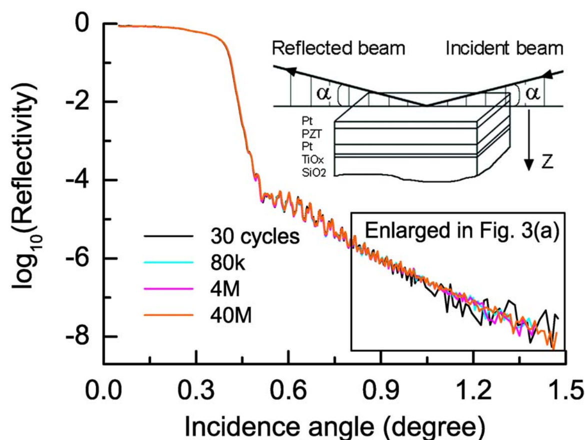

FIG. 2. (Color online) Experimental *in situ* XRSR. The four experimental XRSR curves are measured from the PZT thin film capacitor, corresponding to the four different fatigue states, as shown in Fig. 1. The inset shows the geometry of the thin film capacitor in the x-ray beam during XRSR measurements. With increasing grazing incidence angle α, the electron density profile in deeper layers of the capacitor in the thickness direction Z is accessed by the x rays.

TABLE I. Thickness (d), density (ρ), and surface or upper interface roughness (σ) of the constituent layers in the PZT capacitor obtained from best fits to the experimental XRSR curves. The error margins also indicate qualitatively the maximum differences among the structure parameters during fatigue.

Top Pt	σ (nm)	3.67±0.03
	ρ (g/cm^3)	21.1±0.1
	d (nm)	62.4±0.5
Upper PZT	σ (nm)	1.79±0.03
	ρ (g/cm^3)	7.80±0.05
	d (nm)	93.4±0.3
Lower PZT	σ (nm)	0.6±0.2
	ρ (g/cm^3)	8.00±0.05
	d (nm)	114.2±0.3
Bottom Pt	σ (nm)	1.28±0.05
	ρ (g/cm^3)	20.2±0.5
	d (nm)	97.9±0.2

algorithm[15] using a restricted structure model of homogeneous stratified slabs of top Pt/low-density, PZT/high-density, PZT/bottom, and Pt/TiO_2.[12] Table I gives the global structural parameters including thickness, mass density, and surface or interface root-mean-square roughness of each layer in the capacitor. Thus, the *in situ* XRSR results reveal that essentially no changes to the thickness, mass density, and surface or interface root-mean-square roughness are observable during fatigue. Note here that the roughness is modeled as an error function transition between two materials.

Based on the experimental *in situ* XRSR, theoretical simulations are made to quantify the possible oxygen vacancy accumulation in the PZT thin film capacitor during fatigue. As fatigue occurs to the entire film,[16] a continuous oxygen-depletion layer $Pb(Zr_{0.3}Ti_{0.7})O_{3-\delta}$ between the PZT ferroelectric thin film and Pt top electrode is assumed to simulate the accumulated oxygen vacancies at certain concentrations $[V_O^{\cdot\cdot}]$. The structural parameters of the other layers for the simulations are from best fits to the experimental XRSR. The interface between the oxygen vacancy layer and PZT is assumed to be ideally flat. The mass density of the oxygen vacancy layer differs from that of the PZT sublayer correspondingly because of the oxygen depletion. For simplicity, the distribution of oxygen vacancies in the bulk PZT film is assumed to be homogeneous. Accordingly, the mass density of the PZT sublayers increases due to the oxygen exchange, in order to keep the mass of the PZT layer constant.[17] The sum of the thickness of the oxygen vacancy layer and PZT film remains constant during fatigue to keep consistency with the experimental *in situ* XRSR.

Figure 3(a) shows the region between 0.8° and 1.5° of the experimental *in situ* XRSR curves for the demonstration of the simulation results. This region is the most sensitive to the oxygen vacancy layer assumed for the current case. First, an oxygen-depletion layer $Pb(Zr_{0.3}Ti_{0.7})O_2$ at $[V_O^{\cdot\cdot}]\approx 33.3\%$ is assumed with different thicknesses of $5d_{100}$, $25d_{100}$, and $50d_{100}$ (d_{100}=3.992 Å), as these values have been frequently addressed for the thickness of the oxygen-depletion layer in the literature. Figure 3(b) compares the best fit to the experimental XRSR with the theoretically simulated XRSR. The simulations show that even an ultrathin oxygen vacancy layer of $5d_{100}$ (~2 nm) has strong effects on the XRSR.

Downloaded 11 Feb 2009 to 131.169.95.132. Redistribution subject to AIP license or copyright; see http://apl.aip.org/apl/copyright.jsp

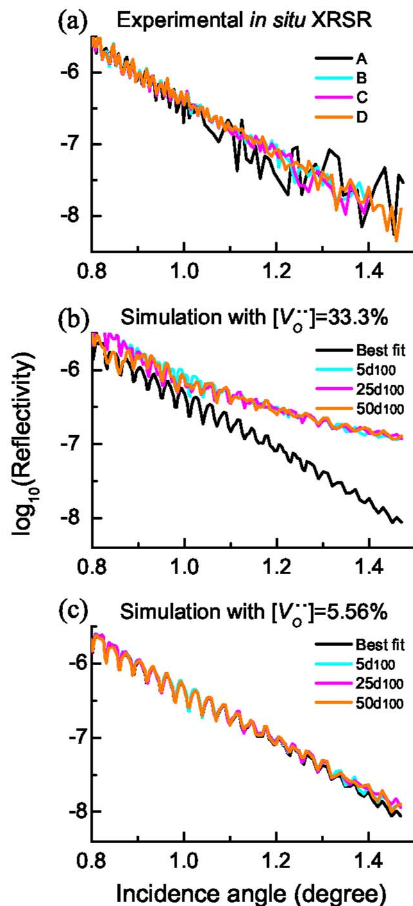

FIG. 3. (Color online) Theoretical XRSR simulations. (a) Experimental XRSR curves between 0.8° and 1.5° enlarged for the demonstration of the simulations. Theoretical simulations for evaluating the possible oxygen vacancy accumulation at the top Pt/PZT interface at different concentrations of (b) 33.3% and (c) 5.56%. The upper $[V_O^{\cdot\cdot}]$ limit for the oxygen vacancy layer at the top Pt/PZT interface is determined to be 5.56%.

However, the appearance of discernible fringes is not sensitive to the exact thickness of the oxygen vacancy layer. Then, an oxygen-depletion layer at smaller $[V_O^{\cdot\cdot}]$ is assumed with different thicknesses. With decreasing oxygen vacancy concentration, the simulated XRSR becomes very close to the best fit.

Figure 3(c) shows the simulated XRSR with a $Pb(Zr_{0.3}Ti_{0.7})O_{2.83}$ layer at an oxygen vacancy concentration of 5.56% for various thicknesses. Thus, the detectable $[V_O^{\cdot\cdot}]$ upper limit of 5.56% at the top Pt/PZT interface is derived [corresponding to $Pb(Zr_{0.3}Ti_{0.7})O_{2.83}$]. Similarly, the $[V_O^{\cdot\cdot}]$ upper limit at the PZT/bottom Pt interface is determined to be 6.67% [corresponding to $Pb(Zr_{0.3}Ti_{0.7})O_{2.80}$]. We obtain the same $[V_O^{\cdot\cdot}]$ upper limits by assuming an oxygen vacancy layer at each of the PZT/Pt interfaces with a typical thickness of $25d_{100}$ (~10 nm).

The experimental *in situ* XRSR reveals that the electron density profile of the ferroelectric layer is modified only very little (if at all) during the fatigue process. Therefore, if fatigue is interface related, the microscopic origin(s) may be rooted in defects related to phase separation[18] or electronic defects[19–21] instead of ionic defects whose accumulation will involve a significant electron density change. Or fatigue in ferroelectric thin films may be body controlled,[22] as the local redistribution of initially random-distributed oxygen vacancies will not affect the electron density profile in the capacitor. Nevertheless, our results do not provide evidence for a fatigue mechanism that involves the long-range migration of oxygen vacancies with subsequent accumulation at the ferroelectric/electrode interfaces. Upper limits of $[V_O^{\cdot\cdot}]$ are given according to theoretical calculations. Whereas we cannot rule out an accumulation of oxygen vacancies below the detection limit, it must be emphasized that such vacancy concentrations are currently believed to be too small to lead to significant fatigue,[8] implying that this fatigue mechanism should be reconsidered.

One of the authors (J.-L.C.) acknowledges support from the Alexander von Humboldt foundation. The authors thank R. Waser, U. Ellerkmann, and P. Gerber for fruitful discussion. They acknowledge partial support from DESY.

[1] J. F. Scott and C. A. Araujo, Science **246**, 1400 (1989).
[2] *Nanoelectronics and Information Technology*, edited by R. Waser (Wiley-VCH, Berlin, 2003), 387.
[3] D. W. Bondurant and F. P. Gnadinger, IEEE Spectrum **26**, 30 (1989).
[4] J. F. Scott, C. A. Araujo, B. M. Melnick, L. D. McMillan, and R. Zuleeg, J. Appl. Phys. **70**, 382 (1991).
[5] K. Yoo and S. B. Desu, Mater. Sci. Eng., B **13**, 319 (1992).
[6] S. Pöykkö and D. J. Chadi, Phys. Rev. Lett. **83**, 1231 (1999).
[7] M. Dawber and J. F. Scott, Appl. Phys. Lett. **76**, 1060 (2000).
[8] J. F. Scott and M. Dawber, Appl. Phys. Lett. **76**, 3801 (2000).
[9] Y. Wang, Q. Y. Shao, and J. M. Liu, Appl. Phys. Lett. **88**, 122902 (2006).
[10] H. N. Al-Shareef, B. A. Tuttle, W. L. Warren, T. J. Headley, D. Dimos, J. A. Voigt, and R. D. Nasby, J. Appl. Phys. **79**, 1013 (1996).
[11] E. Chason and T. M. Mayer, Crit. Rev. Solid State Mater. Sci. **22**, 1 (1997).
[12] J. L. Cao, A. Solbach, U. Klemradt, T. Weirich, J. Mayer, U. Böttger, P. J. Schorn, and R. Waser, Appl. Phys. Lett. **89**, 052901 (2006).
[13] J. L. Cao, A. Solbach, and U. Klemradt, Physica B **357**, 122 (2005).
[14] P. K. Larsen, G. J. M. Dormans, D. J. Taylor, and P. J. Vanveldhoven, J. Appl. Phys. **76**, 2405 (1994).
[15] L. G. Parratt, Phys. Rev. **95**, 359 (1954).
[16] D. H. Do, P. G. Evans, E. D. Isaacs, D. M. Kim, C. B. Eom, and E. M. Dufresne, Nat. Mater. **3**, 365 (2004).
[17] J. Nuffer, D. C. Lupascu, J. Rödel, and M. Schroeder, Appl. Phys. Lett. **79**, 3675 (2001).
[18] X. J. Lou, X. B. Hu, M. Zhang, F. D. Morrison, S. A. T. Redfern, and J. F. Scott, J. Appl. Phys. **99**, 044101 (2006).
[19] K. Tagantsev, I. Stolichnov, E. L. Colla, and N. Setter, J. Appl. Phys. **90**, 1387 (2001).
[20] E. L. Colla, D. V. Taylor, A. K. Tagantsev, and N. Setter, Appl. Phys. Lett. **72**, 2478 (1998).
[21] W. L. Warren, D. Dimos, B. A. Tuttle, R. D. Nasby, and G. E. Pike, Appl. Phys. Lett. **65**, 1018 (1994).
[22] W. L. Warren, B. A. Tuttle, and D. Dimos, Appl. Phys. Lett. **67**, 1426 (1995).

Downloaded 11 Feb 2009 to 131.169.95.132. Redistribution subject to AIP license or copyright; see http://apl.aip.org/apl/copyright.jsp